Analyst

Accepted Manuscript

This article can be cited before page numbers have been issued, to do this please use: M. Tsai, C. Hsiung, Y. Chen, C. Huang, H. Hsu and P. Hsieh, *Analyst*, 2017, DOI: 10.1039/C7AN01374D.

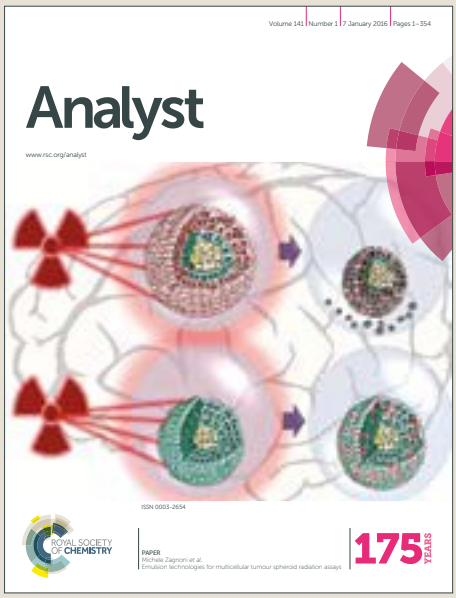

View Article Online
DOI: 10.1039/C7AN01374D

Real-time CRP detection from whole blood using micropost-embedded microfluidic chip incorporated with label-free biosensor

Meng-Zhe Tsai,[a] Chan-Te Hsiung,[a] Yang Chen,[a] Cheng-Sheng Huang,*[a] Hsin-Yun Hsu,[b] Pei-Ying Hsieh[b]

[a]*Department of Mechanical Engineering, National Chiao Tung University, 1001 Ta Hsueh Rd., Hsinchu, Taiwan 30010*
[b]*Department of Applied Chemistry, National Chiao Tung University, 1001 Ta Hsueh Rd., Hsinchu, Taiwan 30010*

**Email:csh@nctu.edu.tw*

Abstract

We demonstrate the detection of C-creative protein (CRP) from whole blood samples without sample pretreatment by using a lab-on-a-chip system consisting of a microfluidic chip and a label-free biosensor. The microfluidic chip includes an array of microposts for filtering blood cells and allows only plasma to flow through and reach the guided-mode resonance (GMR) biosensor for real-time monitoring.

The developed GMR sensor can achieve a bulk sensitivity of 186 nm/RIU, which supports a limit of detection of 3.2 ng/mL for recombinant CRP spiked in human serum. The results are comparable with those obtained using enzyme-linked immunosorbent assay. In addition, we demonstrate the efficacy of filtration of blood cells using microposts and simultaneous measurement of CRP concentration using a GMR sensor by using whole blood and plasma samples.

Introduction

Blood testing is a routine clinical practice for screening or diagnosis of certain diseases by monitoring changes in biomolecules such as proteins and nucleic acids. With few exceptions, preparation of plasma samples from whole blood is a process required for medical diagnosis or analysis[1] to eliminate interference from blood cells, and improving assay sensitivity and reliability. Centrifugation is often used for plasma separation, where the liquid fraction of a whole blood sample can be collected using a pipette. However, centrifugation requires instruments and manual work, which lengthens process time and is prone to human error.

Microfluidic technology or lab-on-a-chip (LOC), which involves the integration of

View Article Online
DOI: 10.1039/C7AN01374D

several functional devices onto the same platform, has shown great potential in simplifying and automating biochemical detection procedures in addition to lowering costs, shortening analysis time, and decreasing the volume of samples required for biological research and clinical applications. For example, Dimov et al. demonstrated on-chip whole blood processing and detection of proteins through fluorescence microscopy.[2]

Label-free (LF) biosensors that can quantify analyte concentrations without requiring fluorescence labels offer many advantages over fluorescence detection and hence have attracted considerable attention.[3] Among different transducing mechanisms, optical LF biosensors are used widely because of their high sensitivity, lack of electromagnetic interference, compact design, simple optical readout, and remote-sensing ability. By monitoring changes in parameters such as wavelength, intensity, and coupling angle, different approaches and apparatus that can quantify the concentration of biomolecules have been demonstrated successfully.[4] Among various optical LF biosensors, surface plasma resonance (SPR) biosensors are the most widely used and investigated. Optical sensors based on guided-mode resonance (GMR; also known as photonic crystal, PC, or resonant waveguide grating, RWG) with higher resolution and a simple readout system have also been commercialized by several companies as desktop-sized biosensor systems. Several research groups have integrated GMR sensors into microfluidic channels[5-7] for various purposes, including miniaturization, fast operation, minimum reagent requirement, and simultaneous quantification; however, none of these groups have included any functional devices in the microfluidic channels. For most optical detection methods based on evanescent field, such as SPR and GMR, it is critical to remove blood cells in order to prevent the interference of cells with the evanescent field. Recently, Jahns et al.[8] included a filter membrane in their microfluidic chip for cell filtration, allowing only plasma to reach the GMR sensor where the imaging mode was used to monitor the intensity variation resulted from the analyte binding. Recently, our group included an array of microposts in a microfluidic chip for filtration of cell debris to allow only in-cell-protein-containing solution to reach GMR sensor for quantification by tracking the shift of the peak wavelength using a spectrometer.

In this work, we demonstrate a LOC system that integrates a microfluidic chip and a GMR biosensor such that the system can filter out blood cells and only allow plasma to reach the biosensor for real-time monitoring. Schematics of the proposed LOC system and the read-out system are illustrated in Fig. 1. The design is based on our previously established LOC system,[9] with modification to the GMR geometry for

View Article Online
DOI: 10.1039/C7AN01374D

higher sensitivity and to the GMR fabrication process for easier assembly with the microfluidic chip.

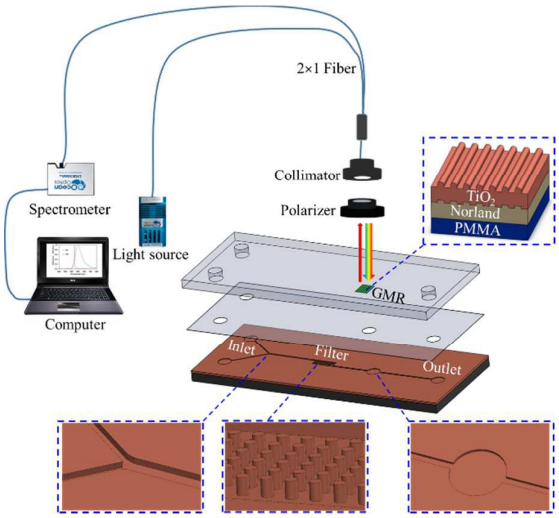

Fig. 1 Schematic of three-layer LOC system and optical read-out setup.

Elevated blood CRP serves as a useful biomarker of acute phase inflammation,[1] tissue necrosis, and trauma.[10] Clinically, it is one of the most valuable acute inflammatory proteins and has been proposed as a potential indicator of bacterial infection which allowed the diagnosis of bacterial sepsis in neonatal infants.[11] High CRP levels in the early stage of bacterial meningitis also indicates high risks in neurological sequelae. Routine CRP measurement facilitates the monitoring of patients' response to antibiotic therapy. Furthermore, CRP values have been assessed in rheumatoid arthritis,[12] systemic lupus erythematosus,[13] vasculitis, inflammatory bowel disease,[14] and myocardial infarction[15] to confirm the validity of CRP for responsive disease diagnostics. CRP detection using LOC systems has been demonstrated, for example, an off-shelf blood filter membrane incorporated into an LOC with innovative capillary-driven microfluidics for CRP detection.[16] However, the device was loaded with serum instead of whole blood, and fluorescence detection was used for the measurement. Aota et al. used a porous membrane to achieve plasma separation.[17] However, they focused mainly on plasma separation. After they obtained the plasma sample, the detection was performed off-chip using microELISA. In the present work, we demonstrate real-time CRP detection from unprocessed whole blood sample as a test model for our LOC system.

Materials and methods

LOC system

View Article Online
DOI: 10.1039/C7AN01374D

The LOC consists of three layers, including a GMR sensor and a microfluidic chip laminated with double-sided tape, as shown in the exploded-view drawing in Fig. 1. First, the sample is loaded into the LOC system from one of the inlets with a syringe. The sample is then flowed through the filter region, where unwanted substances (blood cells in this work) are removed. The analyte is captured by the immobilized ligand on the GMR sensor. By monitoring the resonant wavelength of GMR sensor using the optical setup, the analyte concentration can be determined. Finally, the sample is pumped out via the outlet.

Design and fabrication of GMR sensor

The designed GMR biosensor consists of a one-dimensional surface relief grating structure in a three-layer configuration (see Fig. 1), including a poly(methyl methacrylate) (PMMA) substrate, replicated grating structure on polymer film, and highly refractive index layer of TiO_2.

As demonstrated in previous publications,[18, 19] by increasing the grating period, the bulk sensitivity can be further improved. At the same time, the resonance also shifts towards longer wavelength, which practically limits the choice of optical measurement apparatus. In this work, we have changed the grating period from 400 nm of our previous publication[9] to 555.5 nm, to potentially enhance the bulk sensitivity. Meanwhile, we aimed at resonance within the range that can be observed and detected with typical silicon-based spectrometer and tungsten halogen broadband light source. The fabrication consists of three processes: flexible stamp fabrication (Fig. 2a), replica molding (Fig. 2b–2d), and film deposition (Fig. 2e). First, a silicon (Si) master with grating period, depth, and duty cycle of 555.5 nm, 110 nm, and 0.5, respectively, was purchased from LightSmyth Technologies. We used soft lithography to transfer the grating pattern from the Si master to polydimethylsiloxane (PDMS) (Fig. 2a). Owing to the high aspect ratio and small period of the grating structure, we used hard PDMS (hPDMS) instead of regular PDMS to make the flexible stamp with the replicated grating pattern. The detailed process of fabricating hPDMS can be found in a previous publication.[20] An optical adhesive (NOA 1375, n = 1.375, Norland Products, Inc.) was sandwiched between a PMMA substrate and the flexible hPDMS stamp (Fig. 2b). After the NOA 1375 was cured by exposure to ultraviolet (UV) light (Fig. 2c), the hPDMS stamp was separated from the NOA 1375 (Fig. 2d). A layer of TiO_2 (n=2.22) was then sputtered on top of the NOA 1375 to complete the three-layer GMR sensor (Fig. 2e).

View Article Online
DOI: 10.1039/C7AN01374D

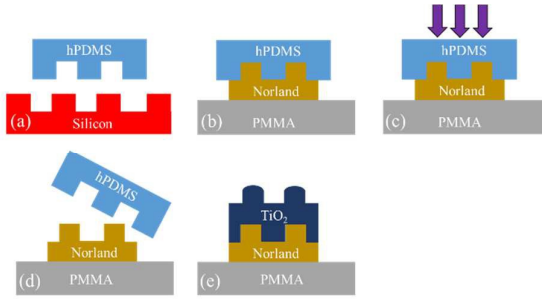

Fig. 2. Fabrication of GMR sensor on PMMA substrate. (a) Replication of grating pattern on hPDMS stamp. (b) Sandwiching of NOA 1375 between hPDMS and PMMA substrate. (c) Solidification of NOA 1375 by UV exposure. (d) Separation of hPDMS from NOA 1375. (e) Sputter deposition of TiO_2 layer.

Scanning electron microscopy (SEM) images of the top and the cross-sectional views of the GMR sensor, shown in Fig. 3, indicated successful replication of the grating structure from the hPDMS stamp to the NOA 1375.

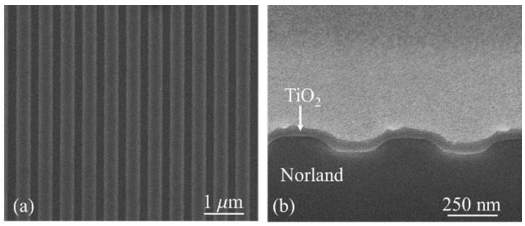

Fig. 3. SEM images of top (a) and cross-sectional (b) views of GMR sensor.

Design and fabrication of microfluidic chip

To automatically remove blood cells for more accurate measurement of the biomolecules, we included an array of microposts in the fluidic channel. The microfluidic channel and micropost filter shown in Fig. 1 were fabricated using SU-8 2035 (negative photoresist, MicroChem Crop.) on a Si wafer through standard photolithography. The detailed fabrication processes can be found in a previous publication.[9] In brief, a layer of SU-8 was spin-coated on top of a Si wafer. After soft-baking to drive out the solvent, a contact aligner was used to transfer the pattern of the fluidic channel and the microposts from a photomask onto the SU-8. Following post-exposure baking after UV exposure, the exposed regions were solidified. The SU-8 was developed in an SU-8 developer to remove the unexposed regions, followed by rinsing with isopropyl alcohol. Lastly, to improve the adhesion and strength of the SU-8, the film was hard-baked.

Integration of microfluidic chip and GMR sensor

The GMR and the microfluidic chip were joined using a double-sided tape (3M

View Article Online
DOI: 10.1039/C7AN01374D

8015P). First, a double-sided tape with an opening hole for the sample to access the GMR sensor was adhered to the GMR sensor. Holes were drilled into both the GMR and the tape for fluid access before bonding with microfluidic chip. Lastly, the tubes were inserted into the access holes and secured with epoxy (8762, LETBOND).

Measurement setup

To measure the reflection spectrum when the sample flowed to the GMR biosensor, the vertical measurement setup shown in Fig. 1 was used. A broadband light source connected to a 2□1 fiber was used to illuminate the GMR sensor at normal incidence. The polarizer was adjusted such that transverse magnetic (TM) polarization was used to excite the device resonance over a narrower line width to achieve higher resolution. The reflection was collected by the same fiber and transmitted to the other end of the 2□1 fiber, which was connected to the spectrometer to monitor the peak wavelength.

Chip preparation for detection of C-reactive protein (CRP)

The GMR was first silanized with epoxy silane (3-glycidoxypropyl-trimethoxysilane) by using vapor phase deposition.[9] 10 μL of 100 μg/mL CRP capture antibodies (MAB17441, R&D Systems) in phosphate-buffered saline (PBS) was applied on the silanized GMR sensor. The antibodies were incubated at 4 ℃ and 95% humidity for 8 h. The GMR sensor was blocked to reduce nonspecific binding by immersion in a 1% solution of casein in PBS at 4 °C for 1 h. Next, the sensor was rinsed using PBS with 0.05% Tween 20 (PBS-T) and deionized (DI) water sequentially before it was attached to the microfluidic channel by using double-sided tape; the tubes were then inserted as described in the integration of microfluidic chip and GMR sensor. The whole microfluidic channel can be blocked to minimize the interaction of analytes with the microfluidic channel surfaces, enabling low concentration measurement and improving the detection limits. Subsequently, the reflection spectrum was measured when the GMR biosensor was filled with PBS, and the reflection peak was used as the baseline signal for any subsequent CRP measurement.

Establishment of CRP calibration curve for LOC system

A standard curve was generated using various concentrations of purified CRP (1744-CR-200, R&D Systems) in 10% human serum in PBS. In total, eight different concentrations ranging from the highest of 50 μg/mL to the lowest of 0.64 ng/mL in 5-fold dilution and one blank (buffer only) were used. Starting from the lowest concentration, the analyte solution was loaded into the LOC system by using a syringe and allowed to incubate for 2 h at room temperature (RT). The system was then rinsed twice by injecting PBS-T to remove the unbound analyte. Next, the PBS was injected

View Article Online
DOI: 10.1039/C7AN01374D

into the LOC before measuring the reflection spectrum. The above procedure was repeated for all concentrations employed herein.

ELISA measurement

To validate the performance of LOC system, we performed conventional enzyme-linked immunosorbent assay (ELISA) in a 96-well microplate by following the protocols specified by the manufacturer (Cat. No. DY1744). Briefly, 10 µg/mL of rat CRP capture antibody was applied to coat the plate. A series of eight standard solutions with known recombinant CRP concentrations (10 µg/mL, 2 µg/mL, 400 ng/mL, 80 ng/mL, 16 ng/mL, 3.2 ng/mL, 0.64 ng/mL, and 0 (buffer only without CRP)) was prepared by 5-fold dilution using PBS with 10% human serum. Following overnight sample incubation, unbound analytes were washed out, and 2 µg/mL of detection antibody (BAM17442, R&D SYSTEMS) was employed for additional 1 h of incubation at RT. Subsequently, horseradish peroxidase (HRP) enzyme was added after washing. At the end of 30 min of incubation at RT, the corresponding substrate TMB was applied to facilitate color reaction (~4 – 30 min). The reaction was stopped using H_2SO_4 (2N), and the absorbance at 450 nm of each sample in the microwell was measured using the ELISA plate reader.

Blood collection and sample preparation

Sprague Dawley rats were purchased from BioLasco Taiwan Co., Ltd and housed in the National Laboratory Animal Center. Whole blood was collected from 12-week-old male rats by tail bleeding and stored in a BD Microtainer Tube Microgard Closure K2EDTA to prevent clotting. Plasma was prepared by centrifugation of fresh blood at 4000 rpm for 10 min at 4 °C to remove blood cells. Care and use of experimental animals in this work complied with the policy and guidelines of the Institutional Animal Care and Use Committee at National Laboratory Animal Center, Taiwan.

Results and discussion

Bulk refractive index sensitivity measurement

As discussed earlier, at normal incidence, a specific wavelength of light is coupled to waveguide modes supported by a higher RI layer (TiO_2) and is reflected backwards. This can manifest as a reflection peak or a transmission dip depending on the measurement setup. The maximum or the minimum intensity corresponding wavelength is the resonant wavelengths of the GMR, which can be calculated using the second-order Bragg condition.[21]

$$\lambda_R = n_{eff}\Lambda \qquad \text{(Eq. 1)}$$

View Article Online
DOI: 10.1039/C7AN01374D

where λ_R is the resonant wavelength, n_{eff} is the effective RI, and Λ is the grating period.

The effective index can be regarded as a weighted average of the RIs of the GMR structure, including TiO_2, NOA 1375, and the sample on top of the TiO_2, which will be altered with the adsorption of biomolecules on the sensor surface. Hence, by monitoring changes in the resonant wavelength, we can determine the amount of biomolecules adsorbed.

Sensitivity refers to the magnitude of the sensor's output response to a given change in sample solution, that is, sample concentration or adsorbed mass density. For optical biosensors, sensitivity is often defined as the ratio of the change in the resonant wavelength to the change in the RI, the unit of which is nm per refractive index unit (RIU)—nm/RIU.

Sucrose solutions of different concentrations—0% (water only) to 60% with an increment of 15%—were used to characterize the bulk sensitivity of the GMR sensor. The sample were loaded into the microfluidic channel by using a syringe, and the reflection spectra were measured using the setup described in the measurement setup. The reflection spectra corresponding to different concentrations are shown in Fig. 4a. The decrease in reflection efficiency with increasing sucrose concentration indicates that absorption increases with increasing sucrose concentration. The full width at half maximum (FWHM) of the reflection spectra ranged between 4.33 to 5.62 nm. Despite the reduced coupling efficiency and broader FWHM compared to the simulation result (Fig. S-2), the reflection peaks were clear enough to be identified for characterization. As suggested by Equation 1, the resonant wavelength increased with increasing effective RI, which increased with increasing RI of the sample solutions. The peak wavelength as a function of the RI shown in Fig. 4b indicates a fairly linear response within the range of the RIs. The performance of our GMR sensor shows a linear response; hence, its sensitivity can be calculated as the slope of the linear fitted line, 186 nm/RIU, which shows improved sensitivity over the previous device,[9] and is comparable to other reported values based on GMR sensors.[18, 22]

View Article Online
DOI: 10.1039/C7AN01374D

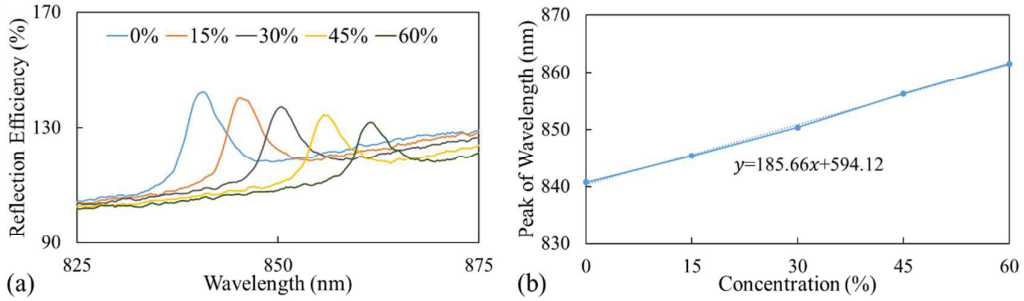

Fig. 4 (a) Reflection spectra obtained using five different sucrose solutions. (b) Peak wavelength as function of RI and linearly fitted line.

CRP detection with LOC chip and ELISA

Purified C-reactive protein detection

The original reflection spectra obtained using different recombinant CRP concentrations in one of the experimental runs are shown in Fig. 5a. With increasing CRP concentration, a larger amount of CRPs can be captured by immobilized CRP capture antibodies, which increases the effective RI, causing the peak (resonant) wavelength to shift to a longer wavelength, as implied by Eq. (1). The original reflection spectra obtained in another two runs are shown in supplementary Figure S-1. The details pertaining to the shifts in the peak wavelength relative to the baseline signal at different concentrations and their corresponding standard deviations for all three experimental runs are also given in supplementary Table S1. The results indicate that the GMR in our LOC is very reliable, and the assay protocol is repeatable. The amounts of average peak wavelength shift relative to the baseline peak (from buffer only sample) as a function of the CRP concentration in all three experimental runs are summarized in Fig. 5b. When the concentration is below 0.64 ng/mL, no shift in peak wavelength can be detected. By contrast, when the concentration is increased to 6.4 ng/mL, a 0.3 nm (minimum differentiable wavelength by our spectrometer) shift in the peak wavelength can be detected. When the concentration is below 10 μg/mL, the peak shift shows a fairly linear relationship with the change in concentration. However, when the concentration is greater than 10 μg/mL, one can see that the amount of peak shift levels off slightly, which could possibly indicate a saturation of binding between the recombinant CRP and the CRP antibodies. This could be further confirmed at higher CRP concentrations; nevertheless, our LOC system shows a dynamic range spanning over five orders of magnitude. To further improve the resolution of peak wavelength shift, two general approaches can be adopted. One can use filtering algorithms such as Savitzky–Golay[23] to smooth the reflection spectrum by reducing the noise. On the other hand, two different curve fitting models (Lorentzian[24] and Fano[22]) are typically used to fit the reflection spectrum, enabling

View Article Online
DOI: 10.1039/C7AN01374D

better reflection peak identification.

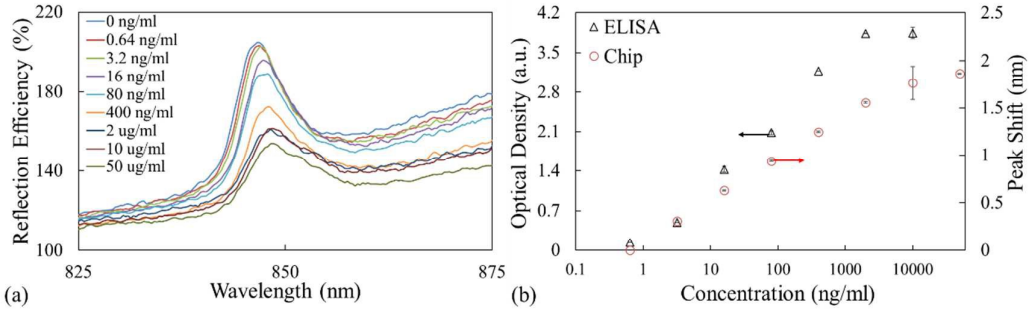

Fig. 5 (a) Original reflection spectra corresponding to different concentrations of recombinant CRP in human serum. (b) Dose-response curves for LOC and ELISA.

The dose response curve obtained using ELISA is shown in Fig. 5b. At 0.64 ng/mL, the optical density (0.134) shows a distinguishable signal (greater than thrice the standard deviation (0.004) of the blank). As the concentration exceeded 2 μg/mL, the output signal remained unchanged (~3.84), which indicates saturation of binding between the antibodies and the CRP. Compared to the dose-response curve obtained using LOC, the ELISA one exhibits a slightly better limit of detection (LOD), but it is saturated more quickly at higher concentrations, which means both measurement techniques have approximately the same detection range.

C-reactive protein detection from whole blood and plasma

In this experiment, we prepared two LOC chips for measuring rat whole blood and plasma samples. Chip fabrication and chip preparation for detecting rat CRP were identical to those used for dose response curve calibration. The reflection spectra were taken as baseline signals, where the CRP antibodies were immobilized on the GMR biosensors and the LOCs were filled with PBS, which were labeled as *antibody* in both Figs. 6a and 6b. Then, the whole blood and the plasma samples were diluted 10 thousand times and incubated on the GMR biosensors for 2 h. The PBS-T was injected into LOCs to rinse the microfluidic channel and to remove the unbound rat CPR and other substances. Lastly, PBS was injected into the LOCs before the reflection spectra were taken. The reflection spectra of the two LOCs loaded with the whole blood and the plasma samples are represented by orange curves in Fig. 6a and 6b, and they are labeled *blood* and *plasma*, respectively. In both Figs. 6a and 6b, the relative shifts from both LOCs are 1.24 nm. In this case, the microposts filter out the cells and the debris effectively and provide the same result for blood and plasma.

View Article Online
DOI: 10.1039/C7AN01374D

By contrast, in the ELISA measurement, the ODs obtained using the whole blood and the plasma samples differ significantly at 2.377±0.067 and 2.605±0.094 respectively. The OD obtained using the whole blood sample was slightly lower than that obtained using plasma. This was possibly because there are a greater number of interferents in the whole blood sample that could potentially nonspecifically block the epitopes of the CRP antibodies to reduce the binding of rat CRP and HRP. This implies that for with ELISA, to obtain consistent measurements, plasma sample preparation is important.

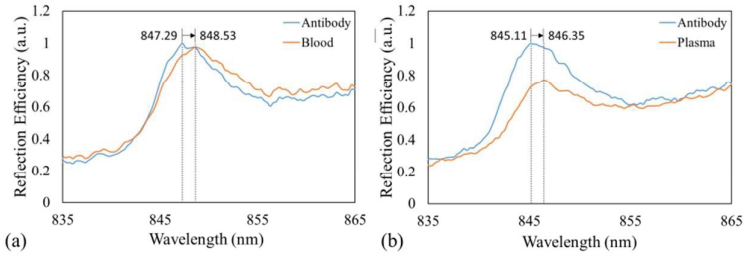

Fig. 6 Reflection spectra of baseline signal (represented with blue curves and labeled as *Antibody*) and reflection spectra after incubation with (a) whole blood and (b) plasma sample.

Verification of filtration by microposts

Injection from outlet

To verify the effect of the array of microposts on the filtration of cells, the same blood and plasma samples were injected from the outlet, such that the samples flowed directly to the GMR biosensor without passing through the filter region. Once the antibodies were incubated on the GMR sensors, PBS was injected and the reflection spectra were taken as the reference signal, as shown by the blue curves and labeled *Antibody* in Figs. 7a and 7b. The whole blood and the plasma samples were injected from the outlet into the LOCs and were incubated for 2 h. Then, PBS-T was used to rinse the LOCs; next, the LOCs were filled with PBS before the reflection spectra were measured, which are shown by orange curves and labeled *Blood* and *Plasma*, respectively. For the blood sample, the peak shifts by about 2.18 nm. However, compared to the result obtained by injecting the sample from the inlet and allowing it to flow through the filter region first before measurement, as shown in Fig. 6a, the peak shifts by only 1.24 nm. The additional peak shift of 0.94 was very likely due to adsorption of cells on the GMR biosensor. This indicates that the cells must be removed to obtain accurate measurements.

By contrast, for the plasma sample, the peak shifts by only about 1.25 nm. In

View Article Online
DOI: 10.1039/C7AN01374D

comparison with the result (peak shift of 1.24 nm) shown in Fig. 6b, this represents a difference of only 0.8%. This was expected because the cells were already removed from the plasma sample; hence, injection from either side should not have affected the

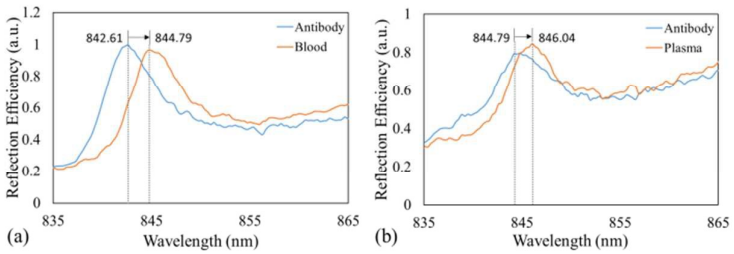

result. Once again, this verifies the consistency of our experimental protocol and GMR sensor chip.

Fig. 7 Reflection spectra of baseline signal (represented by blue curves and labeled *Antibody*) and reflection spectra (brown curves) after incubation with blood (a) and plasma samples (b).

Observation using microscope

To obtain accurate measurements of analyte concentration from blood, often, the sample requires some pretreatment to remove unwanted cells. Hence, plasma samples are preferred. The microscopic images at the entrance from the channel to the micropost region in the cases of plasma and whole blood sample loading are shown in Figs. 8a and 8b, respectively. When the channel is loaded with plasma, there is no sign of cells or other debris trapped in the microposts (Fig. 8a). This was expected because the plasma was already preprocessed to remove cells. The bulges shown in the image could be small air bubbles trapped during sample injection.

The blood cells typically range in size from 7 to 15 μm.[25] In this work, the spacing between the microposts is 6.2 to 6.5 μm, which would prevent the cells from flowing through. This can be verified in Fig. 8b, where the cells are blocked at the onset of the microposts and only the analyte can flow through and reach the GMR biosensor when whole blood is injected into the LOC system. This is why we can obtain the same result from both the whole blood and the plasma samples. However, as shown in Fig. 8b, all cells are blocked only by the first row of the microposts. The layout of and the spacing between the microposts can be optimized to achieve more efficient filtration.

View Article Online
DOI: 10.1039/C7AN01374D

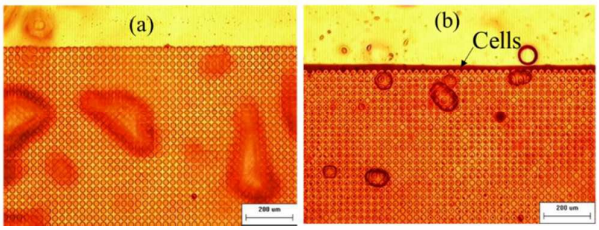

Fig. 8 Microscopic image at entrance of micropost region when (a) plasma and (b) whole blood samples are loaded.

We have developed a GMR biosensor with a bulk sensitivity of 186 nm/RIU and the LOD is ~3.2 ng/mL for recombinant CRP in human serum. Nonetheless, due to the high level of CRP in the blood, the blood was diluted to have its concentration falls within the linear range of quantification. Theoretically, it shall be also feasible for undiluted whole blood when measuring minute amount of other analytes. Due to higher viscosity of undiluted whole blood, potential hemolysis might need to be taken into consideration when higher pressure is required for delivering the sample. Currently, the cells are blocked in the first row, which would increase the flow resistance resulting higher injection pressure for sample delivery. The geometry of micropost array needs to be optimized such that the whole region of microposts can be fully utilized to alleviate the injection pressure for undiluted whole blood sample. For trace analysis, the LOD can be further improved by using a spectrometer of higher resolution or by optimizing the GMR sensor for higher sensitivity. The device can be modified to have multiple GMRs with different capture ligands in series or in parallel to simultaneously detect multiple analytes, enabling better disease diagnostics using a panel of biomarkers. This will be especially beneficial for identification of some complicated hyper-inflammatory syndromes (e.g. SIRS and sepsis)[26, 27] and diverse cancer subtypes [28] to assist physicians for appropriate treatments.

Finally, despite the inexpensive GMR sensor fabricated by replica molding with plastic substrates, the expensive Si substrate for microfluidic chip could prohibit the developed LOC device from disposable applications. We are currently investigating alternative materials and appropriate fabrication processes for microfluidic chips to realize a full plastic LOC device readily applicable in real bedsides of clinics.

Conclusion

In summary, we demonstrate a LOC system combining a microfluidic channel and a GMR biosensor for whole blood sensing. The microfluidic channel consists of an array of microposts capable of filtering blood cells, thus allowing for measurement of analyte from a whole blood sample. As a proof of concept, the detection of rat CRP

View Article Online
DOI: 10.1039/C7AN01374D

from whole blood and plasma were performed with two LOC devices. The same amount of peak shift from GMRs indicates that the microposts can effectively filter out the blood cells allowing only plasma to reach the GMR for accurate detection. This facilitates future point-of-care or handheld devices to directly measure analytes from whole blood samples.

Acknowledgements

This research was supported by the Ministry of Science and Technology (MOST), Taiwan (104-2633-E-009-001-MY2). The authors thank the Nano Facility Center at National Chiao Tung University and National Nano Device Laboratories, Taiwan, for their support in the fabrication and characterization of the GMR sensor and the microfluidic chip. Moreover, the authors also thank Dr. Shang-Yi Chiu for her assistance with the experiment and with writing this manuscript, and the National Laboratory Animal Center for their support preparing the rat whole blood and plasma samples. This manuscript was edited by Wallace Academic Editing.

Reference

1. M. Kersaudy-Kerhoas and E. Sollier, *Lab on a Chip*, 2013, **13**, 3323-3346.
2. I. K. Dimov, L. Basabe-Desmonts, J. L. Garcia-Cordero, B. M. Ross, A. J. Ricco and L. P. Lee, *Lab on a Chip*, 2011, **11**, 845-850.
3. X. D. Fan, I. M. White, S. I. Shopova, H. Y. Zhu, J. D. Suter and Y. Z. Sun, *Analytica Chimica Acta*, 2008, **620**, 8-26.
4. I. M. White and X. Fan, *Optics Express*, 2008, **16**, 1020-1028.
5. C. J. Choi and B. T. Cunningham, *Lab on a Chip*, 2006, **6**, 1373-1380.
6. M. G. Scullion, T. F. Krauss and A. Di Falco, *Sensors*, 2013, **13**, 3675-3710.
7. G. Y. Sung, W.-J. Kim, H. Ko, B. K. Kim, K.-H. Kim, C. Huh and J. Hong, in *Biosensing and Nanomedicine V*, eds. H. Mohseni, M. H. Agahi and M. Razeghi, 2012, vol. 8460, pp. 84600F-84601.
8. S. Jahns, P. Glorius, M. Hansen, Y. Nazirizadeh and M. Gerken, in *Bio-Mems and Medical Microdevices Ii*, ed. S. VanDenDriesche, Spie-Int Soc Optical Engineering, Bellingham, 2015, vol. 9518.
9. Y. K. Tu, M. Z. Tsai, I. C. Lee, H. Y. Hsu and C. S. Huang, *Analyst*, 2016, **141**, 4189-4195.
10. M. B. Pepys and G. M. Hirschfield, *The Journal of Clinical Investigation*, 2003, **111**, 1805-1812.
11. L. Xu, Q. Li, Z. Mo and P. You, *Eur. J. Inflam.*, 2016, **14**, 100-108.
12. C. G. Ammitzboll, R. Steffensen, M. Bogsted, K. Horslev-Petersen, M. L. Hetland, P. Junker, J. S. Johansen, J. Podenphant, M. Ostergaard, T. Ellingsen

View Article Online
DOI: 10.1039/C7AN01374D

and K. Stengaard-Pedersen, *Arthritis Res Ther*, 2014, **16**, 475.

13. H. Enocsson, C. Sjöwall, T. Skogh, M.-L. Eloranta, L. Rönnblom and J. Wetterö, *Arthritis Rheum.*, 2009, **60**, 3755-3760.
14. S. Liu, J. Ren, Q. Xia, X. Wu, G. Han, H. Ren, D. Yan, G. Wang, G. Gu and J. Li, *The American journal of the medical sciences*, 2013, **346**, 467-472.
15. M. B. Clearfield, *The Journal of the American Osteopathic Association*, 2005, **105**, 409-416.
16. L. Gervais and E. Delamarche, *Lab on a Chip*, 2009, **9**, 3330-3337.
17. A. Aota, S. Takahashi, K. Mawatari, Y. Tanaka, Y. Sugii and T. Kitamori, *Anal. Sci.*, 2011, **27**, 1173-1178.
18. I. D. Block, N. Ganesh, M. Lu and B. T. Cunningham, *Ieee Sensors Journal*, 2008, **8**, 274-280.
19. J. Ju, Y.-a. Han and S.-m. Kim, *Sensors*, 2013, **13**, 3232-3241.
20. C.-S. Huang, E. Y.-B. Pun and W.-C. Wang, *Journal of the Optical Society of America B-Optical Physics*, 2009, **26**, 1256-1262.
21. R. Magnusson, Y. Ding, K. J. Lee, D. Shin, P. S. Priambodo, P. P. Young and T. A. Maldonado, in *Nano-and Micro-Optics for Information Systems*, ed. L. A. Eldada, SPIE, Bellingham, 2003, vol. 5225, pp. 20-34.
22. G. J. Triggs, Y. Wang, C. P. Reardon, M. Fischer, G. J. O. Evans and T. F. Krauss, *Optica*, 2017, **4**, 229-234.
23. A. Savitzky, Golay, M. J. E., *Analytical Chemistry* 1964, **36**, 13.
24. N. Ganesh, A. Xiang, N. B. Beltran, D. W. Dobbs and B. T. Cunningham, *Applied Physics Letters*, 2007, **90**.
25. L. Dean, *Blood Groups and Red Cell Antigens [Internet]*, National Center for Biotechnology Information (US), Bethesda, MD, 2005.
26. H.-Y. Hsu, E. M. Schneider, M. Weiss and T. O. Joos, *Med. Eng. Phys.*, 2008, **30**, 976-983.
27. C.-H. Huang, M.-S. Tsai, K.-L. Chien, W.-T. Chang, T.-D. Wang, S.-C. Chen, M. H.-M. Ma, H.-Y. Hsu and W.-J. Chen, *Scientific reports*, 2016, **6**, 27187.
28. N. Schneiderhan-Marra, G. Sauer, C. Kazmaier, H.-Y. Hsu, K. Koretz, H. Deissler and T. O. Joos, *Anal. Bioanal. Chem.*, 2010, **397**, 3329-3338.